

Seeing Statistics at the Upgraded 3.8m UK Infrared Telescope (UKIRT)

Marc S. Seigar¹, Andy J. Adamson¹, Nicholas P. Rees¹, Timothy G. Hawarden²,
Malcolm J. Currie³, Timothy C. Chuter¹

¹Joint Astronomy Centre, 660 N. A'ohoku Place, Hilo, HI 96720, USA

²Astronomy Technology Centre, Royal Observatory, Blackford Hill, Edinburgh, EH9 3HJ, UK

³Starlink, Rutherford Appleton Laboratory, Chilton, Didcot, Oxon, OX11 0QX, UK

ABSTRACT

From 1991 until 1997, the 3.8m UK Infrared Telescope (UKIRT) underwent a programme of upgrades aimed at improving its intrinsic optical performance. This resulted in images with a FWHM of $0''.17$ at $2.2 \mu\text{m}$ in September 1998. To understand and maintain the improvements to the delivered image quality since the completion of the upgrades programme, we have regularly monitored the overall *atmospheric* seeing, as measured by radial displacements of subaperture images (i.e. seeing-generated focus fluctuations), and the *delivered* image diameters. The latter have been measured and recorded automatically since the beginning of 2001 whenever the facility imager UFTI (UKIRT Fast Track Imager) has been in use.

In this paper we report the results of these measurements. We investigate the relation between the delivered image diameter and the RMS atmospheric seeing (as measured by focus fluctuations, mentioned above). We find that the best seeing occurs in the second half of the night, generally after 2am HST and that the best seeing occurs in the summer between the months of July and September. We also find that the relationship between Z_{rms} and delivered image diameter is uncertain. As a result Z_{rms} frequently predicts a larger FWHM than that measured in the images.

Finally, we show that there is no correlation between near-infrared seeing measured at UKIRT and sub-mm seeing measured at the Caltech Submillimetre Observatory (CSO).

Keywords: Telescope optical quality, facility seeing, sub-mm seeing

1. INTRODUCTION

Between 1991 and 1997 the UK Infrared Telescope (UKIRT) was the subject of a systematic campaign of improvements, the UKIRT upgrades programme, which had the explicit goal of providing imaging performance competitive with the best ground-based facilities (Hawarden et al. 1994, 1996, 1998). By active control of the primary-mirror figure and secondary-mirror alignment (Chrysostomou et al. 1998) and tip-tilt actuation of the secondary mirror under control of a fast guider, this goal has been met (Hawarden et al. 1999, 2000). The telescope routinely delivers images with FWHM less than $0''.6$. In 1998 a programme to measure the delivered seeing was undertaken. Images were taken with the Infrared Camera, IRCAM, and the median seeing was found to be $0''.45$. Some images obtained in this programme in September 1998, had a delivered FWHM of $0''.17$.

The new facility imager, the UKIRT Fast Track Imager (UFTI), was delivered at the end of 1998. At the beginning of 2001, a programme to regularly monitor the delivered seeing with UFTI was initiated. In this paper we present results from this programme and compare them with pure atmospheric seeing, as measured from the RMS in the focus position, Z_{rms} .

Further author information: (Send correspondence to M.S.S.)

M.S.S.: E-mail: m.seigar@jach.hawaii.edu, Telephone: (808) 969-6565

2. IMAGE QUALITY

Throughout 2001, UKIRT’s delivered image quality was regularly monitored with UFTI. Whenever UFTI is in use the ORAC-DR imaging pipeline (Economou et al. 1999, Currie 2001) automatically performs photometry on all standard–star frames taken, and a Gaussian fit is used to estimate the FWHM of the central source.

The pipeline calculates the best–fitting elliptical Gaussian point–spread function (PSF) using the Starlink KAPPA (Currie & Berry 2000) package. The PSF task forms marginal profiles at 45°–intervals about the weighted centroid (from task CENTROID) within a 9''2 square. It rejects outliers from any neighbouring sources by ensuring that the intensity declines radially, and excludes bad pixels. For each profile, PSF fits a Gaussian curve, iteratively solving normal equations after background (lower quartile) subtraction. The combined profiles yield approximate values for the Gaussian width, axis ratio and orientation. PSF averages the pixel data into isophotal elliptical annuli about the star image centre. Iterative ellipse fitting generates the accurate minor–axis FWHM, axis ratio and orientation. The pipeline logs the geometric mean of the major and minor–axis FWHM in arcseconds.

Single–component models like the Gaussian or even the twin–parameter Sérsic function (Sérsic 1968) are poor representations of the UKIRT point–spread function under excellent seeing conditions (see the UKIRT web pages, <http://www.jach.hawaii.edu/JACpublic/UKIRT/telescope/telescope.html>). Even in poor conditions the Gaussian overestimates the width of the spiky inner core. Nevertheless, for monitoring performance over a period, the Gaussian FWHM offers a simple, easily interpreted statistic.

The results are rich in statistical information and are analyzed by a code produced by the authors. In order to avoid extended objects, we only employ observations of UKIRT faint standards. Finally, the code corrects the measurements to their equivalents at 1.0 airmasses and the K band, using standard dependences of the image size on airmass (i.e. seeing at zenith \propto airmass^{-3/5}) and wavelength (i.e. seeing at 2.2 μ m \propto ($\frac{\lambda}{2.2}$)^{-1/5} \times seeing at λ , where λ is measured in μ m; see Sarazin & Roddier 1990).

Table 1. Median delivered image diameter as a function of the time of night in 2001. The standard error on each measurement of the median seeing is typically ± 0.006 .

Hawaiian Standard Time (HST) range (hours)	Median image diameter (arcsec)
18–20	0.79
20–22	0.65
22–00	0.62
00–02	0.59
02–04	0.53
04–06	0.54
06–08	0.69

UT coverage is divided into 5 main bins, each covering 2 hours from 6 to 16 hours UT. Image diameter is distributed into 20 bins, between 0'' and 2''. The resulting histograms are shown in Figure 1, along with a plot of image diameter versus UT through the night. Table 1 also shows the median image quality for each UT bin and two extra UT bins at the beginning and end of the night. The additional bins, at HST 18–20 hours and HST 06–08 hours, both represent significantly smaller populations than the other UT bins and so their histograms are not shown in Figure 1.

These data show clearly the variation of image quality through the night. The histogram for the UT range 6–8 hours (HST 20–22 hours) in Figure 1 shows that by this time, the delivered image diameter has essentially stabilized, helped by the dome ventilation system. As the night progresses, the image quality gradually improves

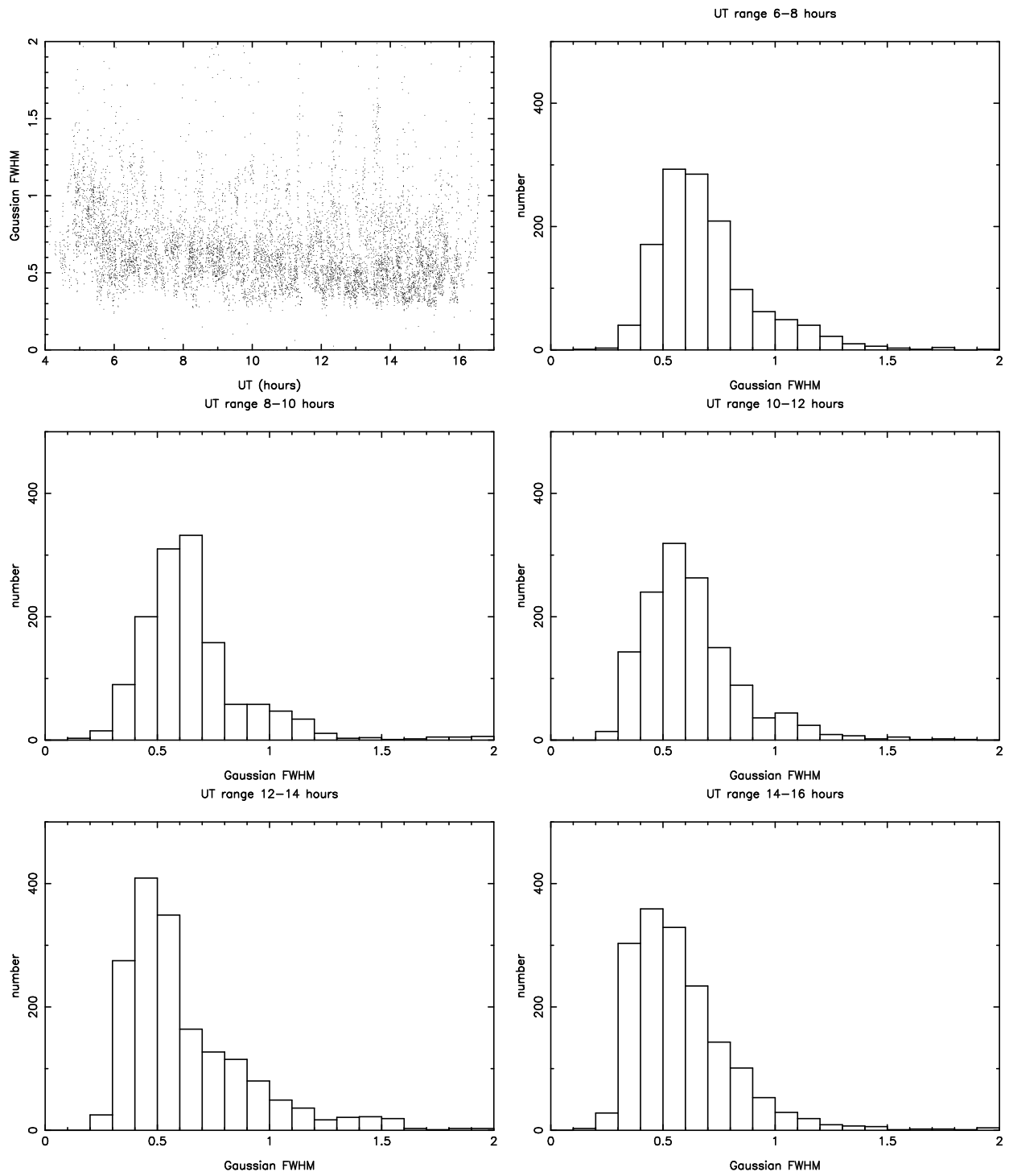


Figure 1. Delivered image diameter versus time of the night, point by point (top left) and in histogram form.

Table 2. Shows how often the delivered image diameter was better than a particular value, e.g. in January the image diameter was better than $0''.3$ 0.48% of the time, better than $0''.4$ 3.8% of the time, better than $0''.5$ 19.8% of the time, etc. The last column lists the median seeing for that month. Data taken earlier than 6 hrs UT are excluded.

Month	Seeing (arcsec)					Median Seeing (arcsec)
	≤ 0.3	≤ 0.4	≤ 0.5	≤ 0.6	≤ 0.7	
Jan	0.48%	3.8%	19.8%	41.8%	61.6%	0.63
Feb	0.52	8.8	23.5	44.6	64.5	0.63
Mar	0.80	1.2	6.8	20.1	45.6	0.71
Apr	0.42	9.6	32.7	62.7	78.4	0.57
May	1.09	9.0	34.0	59.2	74.0	0.58
Jun	0.00	5.3	20.2	37.2	54.3	0.63
Jul	1.71	15.2	32.3	57.8	75.8	0.56
Aug	2.84	27.3	49.0	64.1	79.7	0.50
Sep	0.29	11.7	40.8	63.3	81.0	0.53
Oct	1.09	9.4	20.7	29.7	36.6	0.82
Nov	6.66	45.0	70.8	92.5	99.2	0.49
Dec	0.00	2.2	11.2	27.7	46.0	0.74
All	1.24	12.6	31.1	52.6	69.8	0.60

further. The best image quality is most often observed after 2am HST (12am UT). The histogram representing the UT range 12–14 hours demonstrates this clearly, with the counts quickly rising to $0''.5$, and then tailing off slowly. The median delivered image diameter for this time of the night drops to approximately $0''.53$ (see Table 1).

Table 2 shows seasonal variations in the image quality. Each number in the table represents the percentage of each month for which the delivered FWHM was below a given value. August stands out as the best month, with delivered FWHM being better than $0''.5$ 49% of the time. July and September follow August as the next best months. At face value, November seems to be anomalous; but UFTI was rarely used during November, and then only towards the end of the month when conditions were very good.

The overall median image diameter for 2001, measured by Gaussian fitting as described above, was $0''.6$. While comparisons between these data and those obtained during the 1998 seeing campaign with IRCAM are probably invalidated by the use of different instrumentation, different methods of measuring the image quality (and of course the different epoch), there are some similarities, notably the distinct improvement in late summer.

3. ATMOSPHERIC SEEING

Focus excursions measured by the autofocus system are a measure of atmospheric seeing. Standard atmospheric theory predicts that the seeing-induced image diameter is linearly related to the RMS atmospheric-induced focus fluctuations, Z_{rms} . In this mode, the fast guider is acting as a form of Differential Image Motion Monitor (DIMM). Z_{rms} should therefore be a robust and invaluable measure of the atmospheric seeing (as opposed to delivered image quality) at UKIRT.

The value of Z_{rms} is measured every time the telescope is focussed. During focussing, the Fast Guider re-images the telescope focal plane on the CCD using one of two lens systems mounted in a wheel. A single lens is employed for Normal Guide, Acquisition and Focus modes. For auto-focus a second, similar lens is equipped with a 2×2 array of 4 f/100 Shack–Hartmann lenslets mounted immediately behind it. Instead of a single image these produce 4 images of the star, in a plane somewhat nearer the lens wheel than the single image used for normal guiding.

The longitudinal position of the image formed by the front lens on its own depends on the overall focus of the telescope. Consequently the diameter of the converging pencil in any plane between the lens and its image is a measure of the telescope focus. The four sub-images are formed from sub-pupils of the converging cone

from the single lens, so the radial separation of the four images is also a measure of the overall telescope focus setting. In auto-focus mode the four images are sensed by a 24×24 array of pixels, which are again binned up 3×3 , now into 8×8 superpixels forming four (rather than one) 4×4 guiding arrays.

In autofocus mode the image positions are sensed at a rate of 60 Hz. These measurements are averaged over a specified interval, during which the RMS of the focus fluctuations, Z_{rms} , is also determined. Because the 4×4 sensor is non-linear at large excursions, such as might accompany a change of instrument, when autofocus mode is initiated the 60-Hz focus corrections are averaged, and then applied, over consecutive periods of 2, 4, 8, 16 and 32 seconds, first to facilitate convergence and then to allow seeing-induced fluctuations to be averaged out. The 32s averaging is then repeated indefinitely, until Z_{rms} is seen to stabilise.

To convert Z_{rms} to atmospheric seeing the transformation shown in Equation 1 is used. In Equation 1, the diffraction limit, $0''.15$ is added in quadrature with the contribution from Z_{rms} to give the atmospheric seeing.

$$FWHM = \sqrt{0.15^2 + (28.5Z_{rms}^{6/5})^2} \quad (1)$$

This equation is partly empirical, as the factor of 28.5 was measured by directly comparing delivered image diameter with Z_{rms} over 2 nights from 1999 July 29–30, when a single bright star was imaged in the K band while simultaneously guiding in autofocus mode. The data from these two nights can be seen in Figure 2.

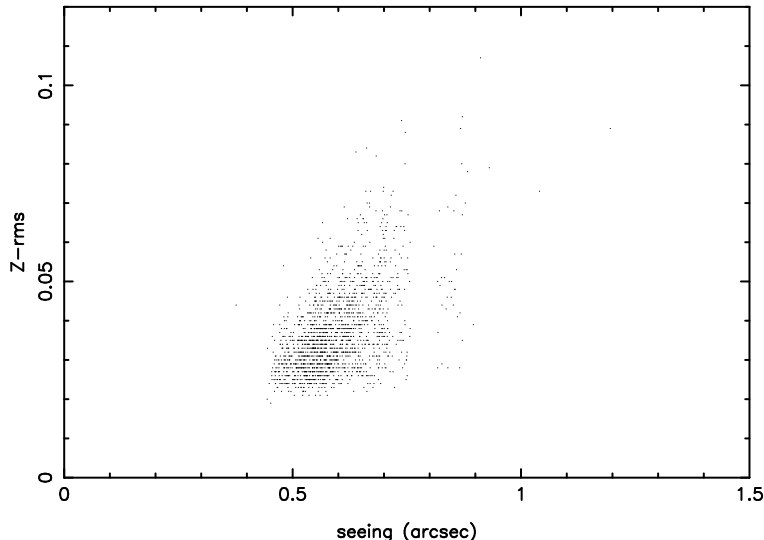


Figure 2. Z_{rms} versus atmospheric seeing for the nights of 1999 July 29–30. A fit to these data results in the factor of 28.5 present in Equation 1.

Using this transformation we have performed a similar analysis to that outlined in Section 2, in order to see how well Z_{rms} relates to the actual delivered seeing. In this analysis we have selected values of Z_{rms} from 2001, in order to remain consistent with the analysis of the delivered UFTI images. The Z_{rms} logfile contains no airmass information, and so the computed atmospheric seeing was not corrected to zenith, although this is a small effect for all but extreme airmasses.

Once again, UT coverage is divided into 5 bins. The resulting histograms are shown in Figure 3, along with a plot of atmospheric seeing versus UT through the night. Table 3 also shows the median seeing for each UT bin and one extra UT bin at the beginning of the night.

These data show how atmospheric seeing (as inferred from Z_{rms}) varies through the night, although this is clearly different from the delivered image quality. At all UT, the atmospheric seeing values have a significantly larger spread than the delivered FWHM. There is some evidence that the histograms are double peaked, except

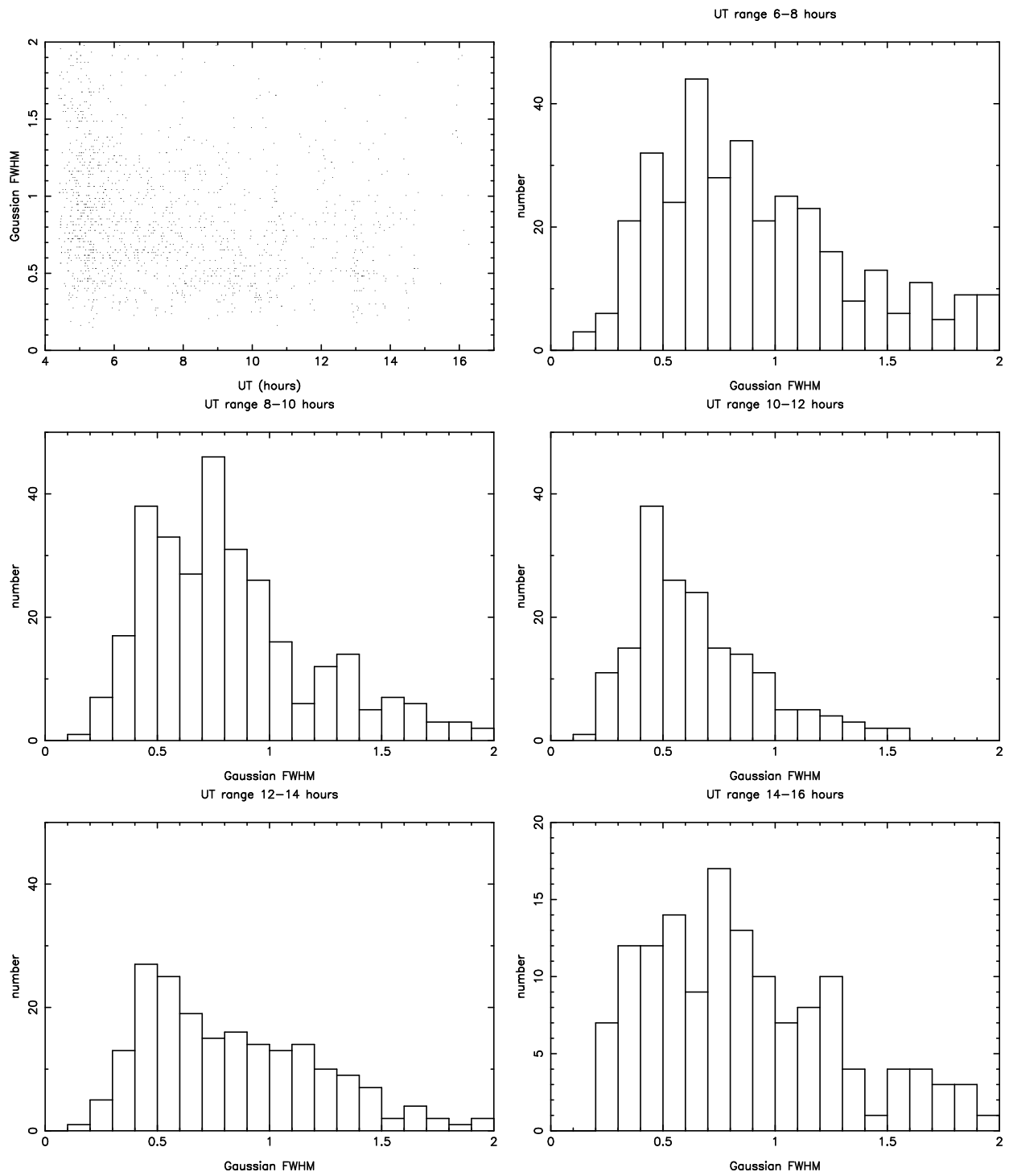


Figure 3. *K* band seeing FWHM inferred from Z_{rms} versus time of the night, point by point (top left) and in histogram form.

Table 3. Median atmospheric seeing as a function of the time of night.

HST range (hours)	Median seeing (arcsec)
18–20	0.93±0.03
20–22	0.82±0.02
22–00	0.76±0.02
00–02	0.58±0.02
02–04	0.76±0.03
04–06	0.78±0.04

in the UT range from 10 – 12 hours. Even the median atmospheric seeing shown in Table 3 does not show the same trend as the delivered seeing. In this case, the median does not slowly decrease through the night while the dome and telescope structure are cooling. Instead a minimum is reached at 10 – 12 hours, but then there is a sharp increase. The overall inferred atmospheric seeing for 2001 was approximately 0''8, significantly larger than the delivered image FWHM of 0''6.

4. DISCUSSION

As discussed in Section 3 there is a theoretical link between Z_{rms} and seeing. Therefore, the delivered image quality should be linked to the value of Z_{rms} in some way as well. Measuring a diameter of a star in a delivered image is not an estimate of the seeing. Faults in the optical system of both the telescope and instrumentation will degrade the best possible image by some degree. One would therefore expect the FWHM of delivered images to be worse than the FWHM estimated from Z_{rms} . We would therefore, expect Figures 1 and 2 to look similar, but with Figure 1 having a *higher* median value for each histogram than Figure 2. This does not seem to be the case. The FWHM inferred from Z_{rms} has both a larger median and scatter than that measured in the delivered images.

When plotting the FWHM in the delivered images against Z_{rms} , reasonable agreement is found with Equation 1. In Figure 5, the mean Z_{rms} has been plotted versus 11 seeing bins (0''3–0''4, 0''4–0''5 etc). This shows that, although there is a large scatter in the value of the inferred seeing FWHM from Z_{rms} compared to the delivered image FWHM (see Figures 1 and 3), the mean value of Z_{rms} in a large dataset tends towards value predicted by Equation 1. This suggests that the calibration used to predict Equation 1 is approximately correct. However, the large scatter in Z_{rms} is still a problem, especially for flexible scheduling where the value of Z_{rms} is often the quickest and simplest way of flexing against the seeing. The cause of the larger median discussed above is the long tails seen in the distributions of inferred atmospheric seeing in Figure 3.

The intra-night variations for both the delivered FWHM and the Z_{rms} inferred FWHM have minima at some time after midnight. Table 1 shows that the delivered FWHM has a minimum value of 0''53 between 12–14 hours UT, rising to 0''54 between 14–16 hours (although this rise is not statistically significant). The minimum for atmospheric seeing occurs slightly earlier in the night, with a value of 0''58 between 10–12 hours UT, and then a sharp rise to 0''76 between 12–14 hours.

Figure 5 shows a plot of median delivered image FWHM versus the month of the year for both 2000 and 2001. The statistics in Table 2, suggested that November 2001 was a very good month, but there were only a few nights available for observing in November 2001, due to bad weather conditions. It seems that the nights that were not affected by the weather were anomalously good for that particular time of year. The best seeing for both years falls around the same time of year, i.e. from July to September. This is consistent with the 0''17 seeing images achieved at UKIRT in September 1998 with IRCAM. In 2000 a gradual increase is seen between the best months and November, whereas a discontinuous variation is seen between September and November

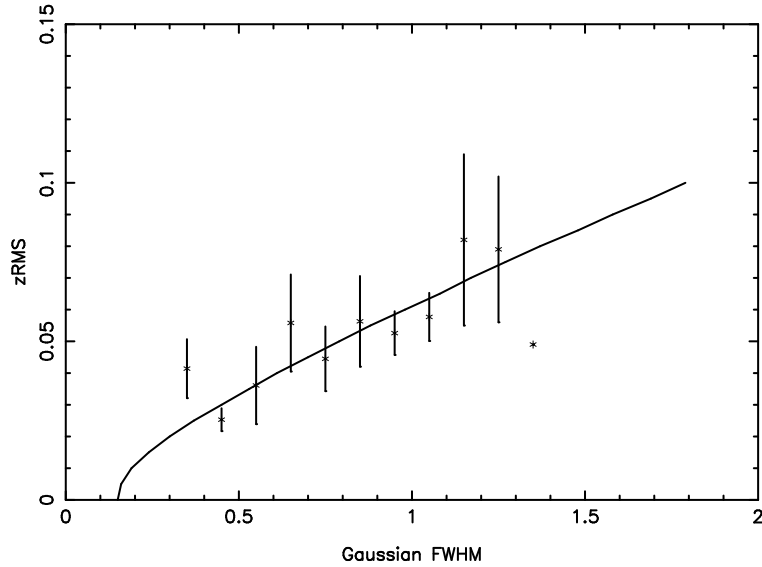


Figure 4. Z_{rms} versus FWHM in delivered images. The line represents the theoretical link between Z_{rms} and atmospheric seeing described by Equation 1. The error bars are one standard error.

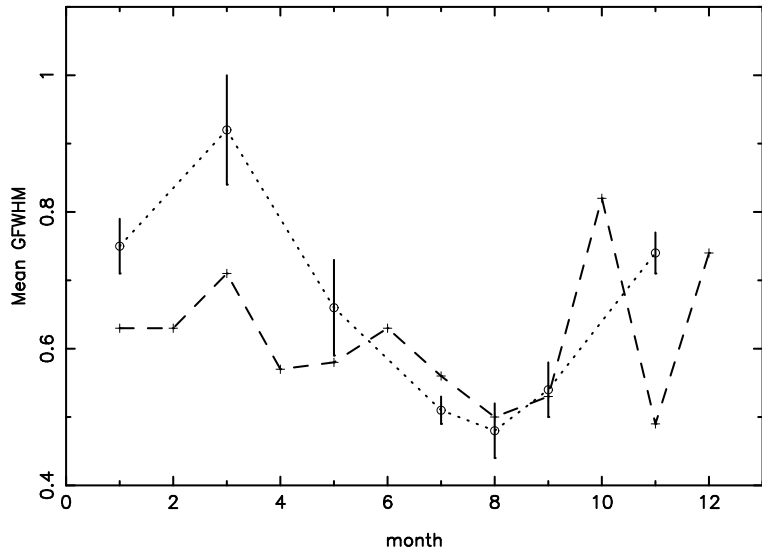


Figure 5. Median delivered image quality versus month of the year (1=January, 2=February, 3=March etc). The dotted line represents 2000, with circles representing the data for 2000. The dashed line represents 2001, with crosses representing the data for 2001. The error bars on the data from 2001 are very small due to the large amount of data compared with 2000.

in 2001. This suggests that, as previously thought, November 2001 was anomalously good. There is anecdotal evidence to suggest that very good seeing can occur directly after a storm, and this may be what we are seeing in November 2001.

Finally we have investigated the relationship between CSO submillimetre seeing and near-infrared K-band seeing. We chose two nights on which to compare these quantities, both of which were nights devoted to observations of UKIRT faint standards. The first night, 2001 March 4th, was particularly bad for IR seeing. The second night, 2001 August 14th, was particularly good for IR seeing. The measurements of IR seeing and

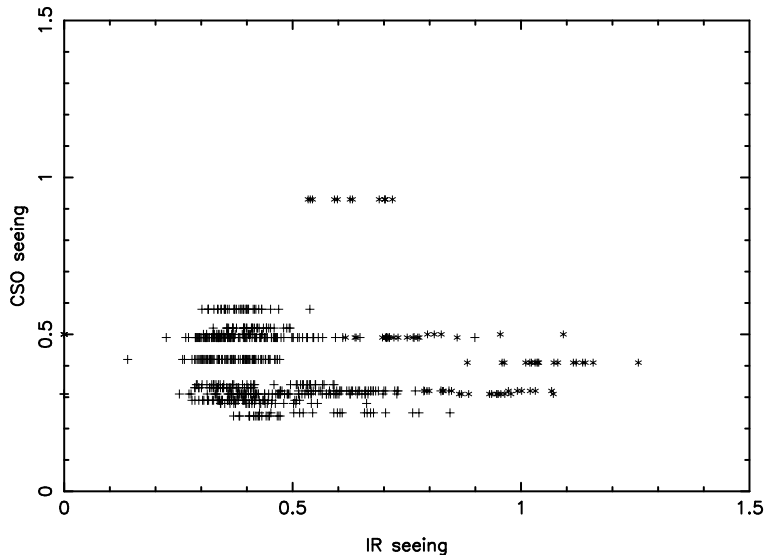


Figure 6. CSO submillimetre seeing versus near-infrared K-band seeing. The stars represent data taken on 2001 March 4th, which was a particularly bad night for infrared seeing. The crosses represent data taken on 2001 August 14th, which was a particularly good night for infrared seeing. In this plot, there are several measurements of IR seeing for every measurement of CSO seeing.

CSO seeing for these nights are plotted in Figure 4, which shows no correlation between these two quantities. This is not surprising since submillimetre seeing depends mainly on water vapour, whereas near-infrared seeing depends on atmospheric conditions such as wind shear.

5. CONCLUSIONS

The main conclusions of this work are summarized as follows:

- The best seeing occurs in the second half of the night, generally after 2am HST.
- The best seeing occurs in the summer, between the months of July and September. This seems to be consistent with both 2000 and 2001, and also 1997, when seeing of $0''.17$ was achieved in September.
- The relationship between Z_{rms} and delivered image diameter is uncertain. When mean Z_{rms} is plotted versus seeing bins, the relationship between the two fits the empirical model quite well. Therefore, for a large dataset, the mean value of Z_{rms} agrees well with the inferred seeing, but in an individual measurement, the inferred seeing can disagree with the measured image FWHM by up to $\sim 40\%$, due to the large scatter in Z_{rms} with respect to the delivered image diameter. This impacts on how one uses Z_{rms} to predict the seeing with a flexibly scheduled telescope.
- There is no correlation between CSO submillimetre seeing and near-infrared seeing.

ACKNOWLEDGMENTS

The United Kingdom Infrared Telescope is operated by the Joint Astronomy Centre, and Starlink is managed by the Council for the Central Laboratory for the Research Councils, both on behalf of the U.K. Particle Physics and Astronomy Research Council.

REFERENCES

1. Chrysostomou, A.C., Rees, N.P., Hawarden, T.G., Cavedoni, C.P., Pettie, D.G., Bennett, R.J., Atad-Ettedgui, E., Humphries, C.M., & Mack, B., 1998, *Active optics at UKIRT*. Proc SPIE, 3352, 446
2. Currie, M.J., 2001, Starlink User Note 232
<http://www.starlink.rl.ac.uk/star/docs/sun232.htx/sun232.html>
3. Currie, M.J., & Berry, D.S., 2000, Starlink User Note 95
<http://www.starlink.rl.ac.uk/star/docs/sun95.htx/sun95.html>
4. Economou, F., Bridger, A., Wright, G.S., Jenness, T., Currie, M.J., & Adamson, A.J., 1999, in ASP Conf. Ser., Vol. 172, *Astronomical Data Analysis Software and Systems VIII*, eds. D.M. Mehringer, R.L. Plante, & D.A. Roberts (San Francisco: ASP), 11
5. Hawarden, T.G., Cavedoni, C.P., Rees, N.P., Chuter, T.C., Pettie, D.G., Humphries, C.M., Bennett, R.J., Atad, E., Harris, J.W., Mack, B., Pitz, E., Glindeman, A., & Rohloff, R.-R., 1994, *The UKIRT Upgrades Programme: Preparing for the 21st Century*. Proc SPIE, 2199, 494
6. Hawarden, T.G., Cavedoni, C.P., Chuter, T.C., Look, I.A., Rees, N.P., Pettie, D.G., Bennett, R.J., Atad, E., Harris, J.W., Humphries, C.M., Mack, B., Pitz, E., Glindeman, A., Hippler, S., Rohloff, R.-R., & Wagner, K., 1996, *Progress of the UKIRT Upgrades Programme*. Proc SPIE, 2871, 256
7. Hawarden, T.G., Rees, N.P., Cavedoni, C.P., Chuter, T.C., Chrysostomou, A.C., Pettie, D.G., Bennett, R.J., Atad, E., Harris, J.W., Mack, B., Pitz, E., Glindeman, A., Hippler, S., Rohloff, R.-R., & Wagner, K., 1998, *The Upgraded UKIRT*. Proc SPIE, 3352, 52
8. Hawarden, T.G., Rees, N.P., Chuter, T.C., Chrysostomou, A.C., Cavedoni, C.P., Rohloff, R.-R., Pitz, E., Pettie, D.G., Bennett, R.J., & Atad-Ettedgui, E., 1999, *Post-Upgrade Performance of the 3.8m UK Infrared Telescope (UKIRT)*. Proc SPIE, 3785, 82
9. Hawarden, T.G., Adamson, A.J., Chuter, T.C., Rees, N.P., Massey, R.J., Cavedoni, C.P., & Atad-Ettedgui, E., 2000, *Thermal Performance and Facility Seeing at the Upgraded 3.8m UK Infrared Telescope (UKIRT)*. Proc SPIE, 4004, 104
10. Sarazin, M., & Roddier, F., 1990, *The ESO differential image motion monitor*. A&A, 227, 294
11. Sérsic, J.-L., 1968, *Atlas de galaxias australes* (Observatorio Astronomica, Cordoba)